SEAWATER $^{87}SR/^{86}SR$ STRATIGRAPHY OF THE MIDDLE ORDOVICIAN IN CENTRAL VIRGINIA

Undergraduate Research Thesis
Submitted in Partial Fulfillment of the requirements for graduation
with honors research distinction in Earth Sciences
in the undergraduate colleges of
The Ohio State University

By

Sean M. Newby
The Ohio State University
May 2017

Approved by

Matthew R. Saltzman, Advisor

School of Earth Sciences

TABLE OF CONTENTS

Abstract

Throughout most of the past century, the correlation of strata in a region has mainly been defined through biostratigraphy, the dating of rock through fossil succession. However, work over the past several decades has put increasing emphasis on dating rock formations through chemostratigraphy. This process utilizes secular trends in ancient seawater chemistry preserved in fossils and rocks, which can, in some cases, provide more accurate dating of strata. This project utilized the $^{87}Sr/^{86}Sr$ seawater curve and existing $\delta^{13}C$ data to more accurately date the New Market Formation and underlying Knox Unconformity in central Virginia, which are approximately Middle Ordovician in age (~470–458 mya). The age of the New Market Formation has been studied previously near Collierstown, Virginia, primarily through conodont biostratigraphy. The Knox Unconformity forms the base of this formation. This major erosional unconformity occurs through much of eastern North American and represents a fall in relative sea level, and with this work, can be dated at Collierstown to terminate around 462.5 Ma. The cause of this unconformity is either through cooling climate that lowered sea level or regional tectonic uplift and mountain building raising the seafloor above sea level. This Sr isotope study suggests that sea-level changes are more effectively correlated to the unconformity, but the presence of regional uplift is still an important feature towards understanding the processes occurring. Either can have major ramifications for the development of life on Earth around this time, and a more accurate date for this unconformity can better explain the sequence of events that spurred one of the major adaptive radiations in history, the Great Ordovician Biodiversification Event (GOBE), a major ecological change related to the rise of the Paleozoic fauna.

Acknowledgements

I would like to thank Matt for providing me with the basis for this work, for his help at Collierstown, and especially for his knowledge on stable isotopes and the Ordovician. I also would like to thank Stig Bergström for teaching me so much about conodonts. Thank you very much to Deanna, Jeff, and Cole for teaching how to work in the clean lab, run the mass spectrometer and answering my questions relating to the lab. Furthermore, I would like to thank Jeff for all of his help in fixing the mass spec whenever a problem came up. I want to thank Mark Kleffner for aiding in the heavy-liquid separation of my samples. In addition, I am extremely grateful to the Friends of Orton Hall Fund for providing me with funding through different parts of my research and the Undergraduate Research Office for the Undergraduate Research Scholarship during my final year of research. I want to thank the School of Earth Sciences for providing me with the Joan Echols Scholarship and Ohio State for their Maximus Scholarship.

List of Figures

List of Tables

INTRODUCTION

The Ordovician was a period of major changes in the evolution of animal life, which began with one of the largest biodiversification events in Earth history and ended with a mass extinction. These events, the Great Ordovician Biodiversification Event (GOBE) and the end-Ordovician (Hirnantian) extinction event, respectively, have major implications on the development of early complex animal life (Sepkoski, 1995). This thesis is primarily concerned with the former, which included a rapid rate of speciation in the fossil record and occupied the early to middle part of the Ordovician. Though the Cambrian Explosion represents an impressive increase in the complexity and diversity of animal life, the GOBE signals the rise of the Paleozoic Fauna that filled unoccupied ecological niches (e.g. Sepkoski, 1995; Trotter et al., 2008; Harper et al., 2015). There were many factors involved in the GOBE, which likely included both physical and biological drivers.

One of the more important factors in Ordovician evolution is the global climate, which can aid or hamper the rate of radiation (Trotter et al., 2008). An overall drop in sea surface temperatures throughout the Ordovician has been proposed based on oxygen isotope measurements of conodont apatite (Trotter et al., 2008), but associated changes in sea level that could have played an important role as an evolutionary driver are poorly constrained. During the Ordovician, sea levels were generally rising, reaching the Paleozoic maximum in the Late Ordovician (Haq and Schutter, 2008), but controversy surrounds the relative importance of tectonics and glacial ice volume (Rasmussen et al., 2016). Long-term sea level rise was intermixed with several periods of shorter-term sea-level regressions with associated cooling (Haq and Schutter, 2008), which appears to have additionally aided in diversification through the creation of relatively temperate waters (Trotter et al., 2008). Cooling events and glaciations on a larger scale are also associated with the mass extinction event that marks the end of the Ordovician (Lenton et al., 2012), which further emphasizes the importance of understanding how sea-level changes may affect biodiversity in concert with or independent of temperature change. It should also be noted that changes in sea level itself could have a major impact on biodiversity, such as through the expansion of terrestrial or shallow marine environments during regressions and transgressions, respectively, allowing for the radiation and extinction of groups of organisms (Haq and Schutter, 2008).

One method to understand the timing and magnitude of sea-level change is through the dating of existing unconformities throughout the Ordovician. For shallow marine rocks, falling sea level, which exposes land that was previously submerged, results in characteristic sedimentological evidence such as brecciated beds (Read, 1980; Mussman and Read, 1986; Dwyer and Repetski, 2012). Dating strata below and above the unconformity could provide the maximum duration of the regressive event. By careful dating of the unconformity and comparisons to the global eustatic curve (Haq and Schutter, 2008), it may be possible to sort out whether local uplift played a role in erosion (Dwyer and Repetski, 2012). This is especially important for a period such as the Middle Ordovician, which is known to have included several major tectonic events such as the Taconic Orogeny. These orogenic events are important as they expose new silicate rock that can act as a sink for carbon dioxide (Young et al., 2009). Correlating unconformities of several regions can help explain linkages among sea level, cooling, and orogeny.

The purpose of this study is to date a specific outcropping of the prominent Middle Ordovician Knox Unconformity and compare this to related unconformities worldwide to better determine the processes affecting the Earth system. Biostratigraphy has been the main manner by which to date and correlate the Knox Unconformity (O'Neill, 1985; Holmden et al., 1996; Sweet and Donoghue, 2001; Haq and Schutter, 2008; Bergström et al., 2009). However, in localities where the fossil record is poor or lacks cosmopolitan index species other means are necessary.

An increasingly popular method used to correlate strata is chemostratigraphy (Ainsaar et al., 2010; Cramer et al., 2010; Edwards and Saltzman, 2014; Saltzman et al., 2014). Isotopic curves, such as carbon and strontium, are used for correlation, but they also have implications for climatic, biologic, and geologic processes occurring at the time. One of the more popular curves utilizes carbon isotopes, typically the $\delta^{13}C$ (e.g. Ainsaar et al., 2010; Cramer et al., 2010; Edwards and Saltzman, 2014), to date sections and understand the local and global carbon cycle and how these processes interrelate to the climatic and biologic components of the geologic record (Young et al., 2009; Edwards and Saltzman, 2014). This method of correlation comes with shortfalls, however, as a $\delta^{13}C$ excursion in a local curve can be affected by many variables other than global carbon cycling, which can lead to inaccurate dating (Edwards and Saltzman, 2014). Another curve that has a longer residence time, and therefore is less influenced by local events, is the strontium isotopic curve, measured by the ratio $^{87}Sr/^{86}Sr$ (e.g. Young et al., 2009; MacArthur et al., 2012; Edwards and Saltzman, 2014; Saltzman et al., 2014). This also has issues due to this longer residence time creating less pronounced fluctuations for use in correlation, especially for periods of highly scattered data due to differences between the curves utilized for the global curve, likely due to diagenetic differences (MacArthur et al., 2012).

The use of both chemostratigraphic curves, $\delta^{13}C$ and $^{87}Sr/^{86}Sr$, in order to refine the known biostratigraphy may improve the dating of known unconformities whilst also providing insights into the changes occurring in the world. The dating and correlating of important unconformities may provide insight into what drivers were at play at this time, either eustatic sea level drop or regional tectonic activity. These would have important implications on the model described by Trotter et al. (2008), where cooling temperatures aided in the biodiversity seen in the GOBE.

GEOLOGIC SETTING AND BACKGROUND

Outcrop

The focus of this study is a section exposed at a roadside outcrop near Collierstown, VA. The exposed rock is located along the northern side of the Colliers Creek and Collierstown Road, approximately 10 miles from Lexington, Virginia (Fig. 1). The road-cut is several meters high and capped in large amounts of vegetation, with some of this vegetation coming down onto the outcrop (Fig. 2).

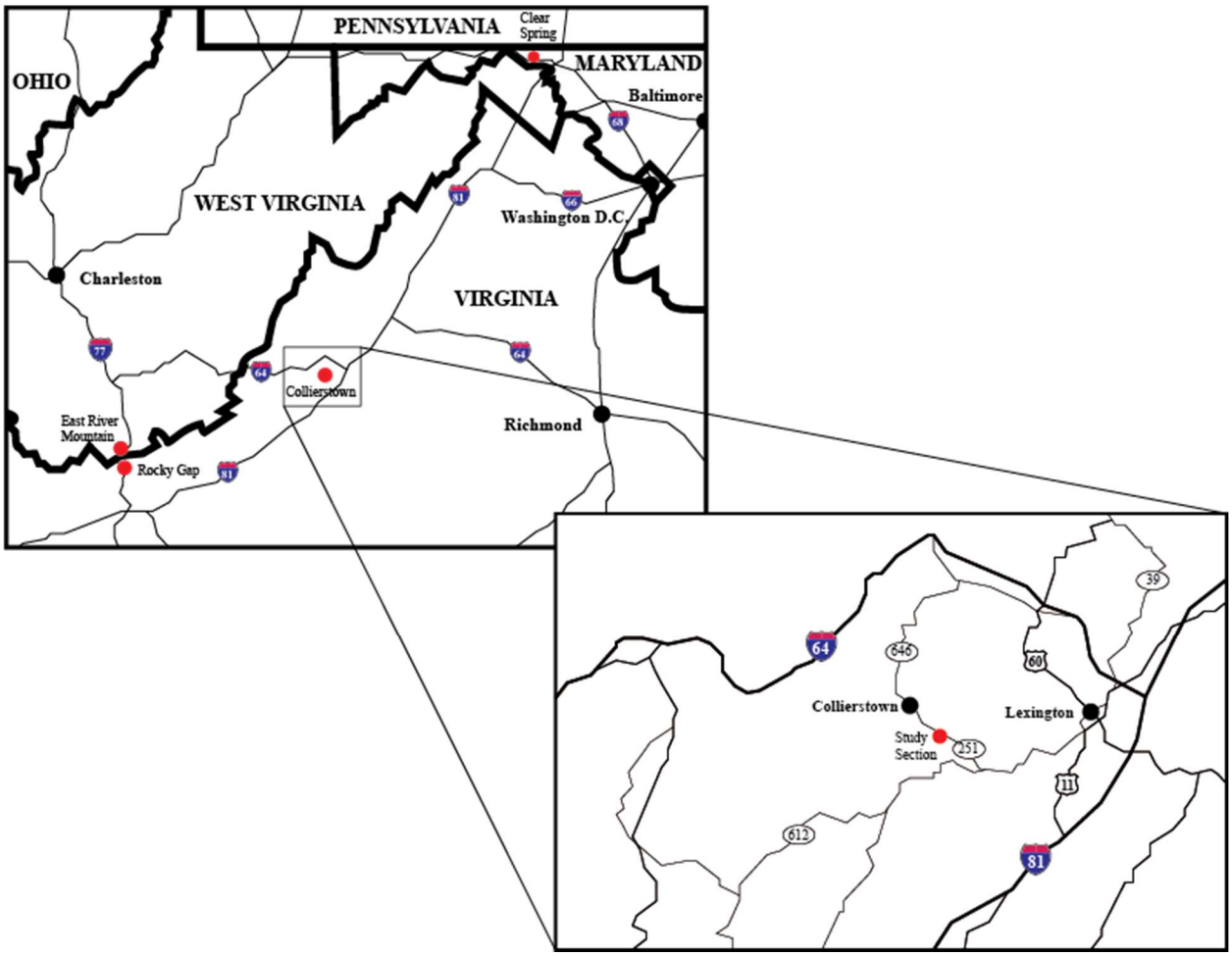

Figure 1: Locality map of sites studied in the Appalachian Valley and Ridge Province, with inset on the focus of this study, Collierstown. Collierstown is located near Lexington, Virginia, near the intersection of Interstates 64 and 81. It is specifically at 37.768344 N, 79.566596 W. East River Mountain and Rocky Gap, two sites visited by other students in past years, are located southwest of Collierstown along the West Virginia-Virginia border. Clear Spring, Maryland is located north along I-81 and is a biostratigraphic and chemostratigraphic reference site for this section of the Appalachian Mountains.

Figure 2: Photographs of the Collierstown Section, highlighting the Knox Unconformity (courtesy of Google Street View). The Beekmantown Dolomite represents material below the unconformity, while the New Market Limestone represents more recent material after a period of non-deposition. The lowest most member of the New Market Limestone, unit 2 (as described by O'Neill, 1985), is a conglomerate consisting of material reworked from the lower Beekmantown Dolomite during the intervening non-depositional period (O'Neill, 1985).

Paleogeography

The Collierstown section is Early to Middle Ordovician in age, during which time this region was part of the partially submerged ancient continent of Laurentia, located near the equator (Blakey, 2011) (Fig. 3). The tectonic setting was a passive margin on which a shallow marine carbonate platform formed (Read, 1980). Carbonate platform deposition was disrupted as the passive margin transitioned into a foreland basin setting during the Taconic orogeny (Read, 1980; O'Neill, 1985). The main purpose of this thesis is to study and date the Knox Unconformity that formed during this transition (O'Neill, 1985; Mussman and Read, 1986; Dwyer and Repetski, 2012).

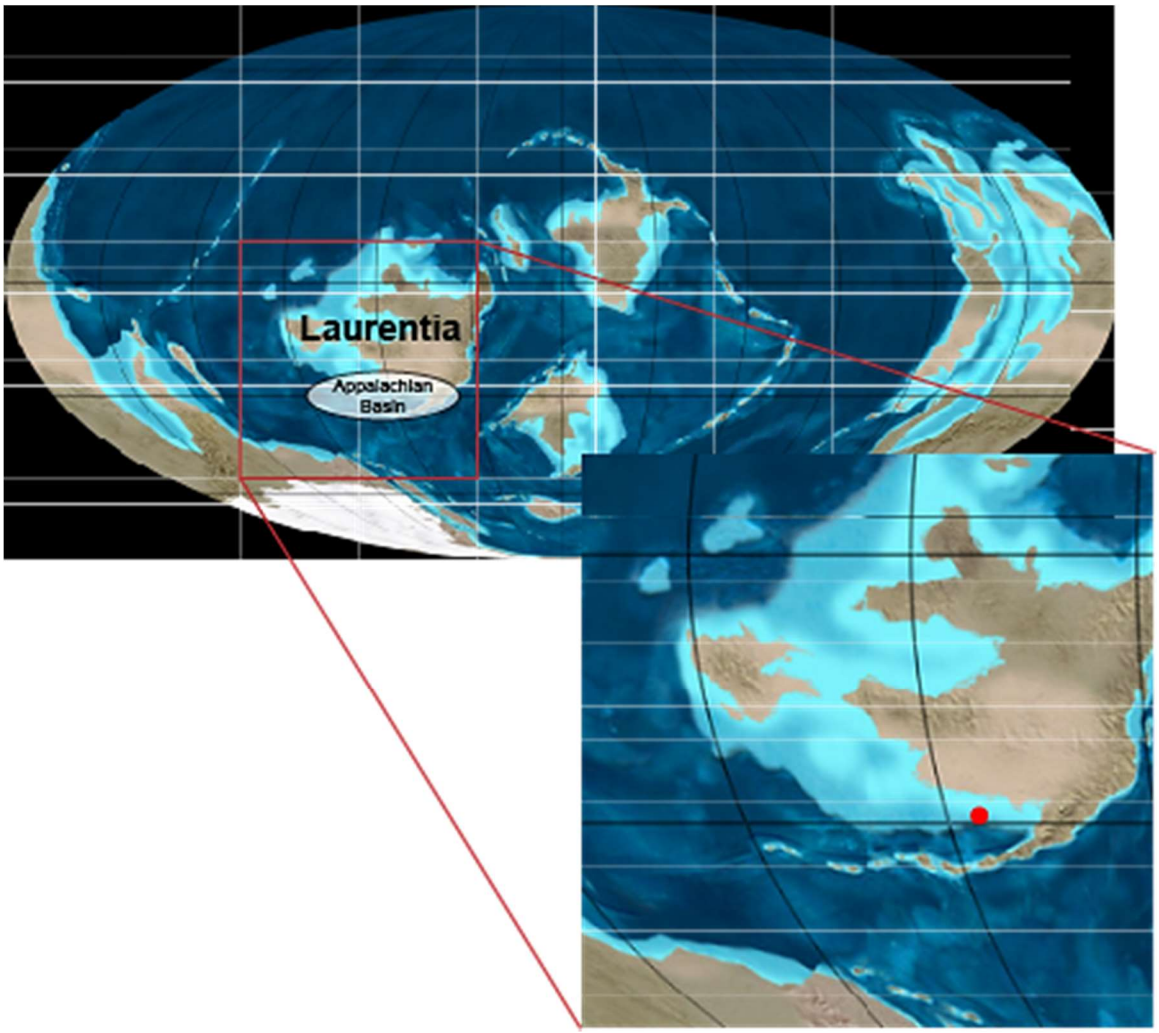

Figure 3: Paleogeographic map of the Middle Ordovician, highlighting the Appalachian Basin of Laurentia (Blakey, 2011). The red dot indicates the location of Collierstown around this time. The Taconic Orogeny is occurring during this period, creating the foreland basin in which the sections described above (Fig. 1) were being deposited (Mussman and Read, 1986).

Lithology

The formations sampled for this project are the Beekmantown Dolomite, New Market Limestone, and Whistle Creek Limestone (Read 1980; O'Neill, 1985). These units are all tilted at approximately 70 degrees. The Beekmantown Dolomite consists of dolostone that abruptly ends at the Knox Unconformity (O'Neill, 1985; see Fig. 2). Above the unconformity, the base of the New Market Limestone is a conglomerate, approximately 1m thick. This consists of material reworked from the lower Beekmantown Dolomite (O'Neill, 1985). The remainder is a fine-grained limestone with chert nodules and calcite veins, both appearing and becoming increasingly more common towards the top of the formation (O'Neill, 1985). The overlying Whistle Creek Formation, which begins 40m above the Knox Unconformity, is a darker gray poorly bedded limestone with frequent interspersed black chert nodules.

Biostratigraphy

Conodont elements can be utilized for biostratigraphy. Conodonts are small marine organisms with apatite-based feeding apparatuses, described as conodont elements. The elements of these eel-like organisms have been preserved in the fossil record throughout most of the Paleozoic and into the Triassic (Sweet and Donoghue, 2001) (Fig. 4). The relative abundance and rapid change in conodonts allow for their use in biostratigraphic analysis of Paleozoic rocks (Bergström et al., 2009). Both shallow-water North American Midcontinent and deeper-water North Atlantic conodonts are found at Collierstown (O'Neill, 1985). Former work done by O'Neill (1985) determined the conodonts found are approximately within the *Pygodus serra* to *Pygodus anserinus* conodont zones of the North Atlantic biogeographic realm.

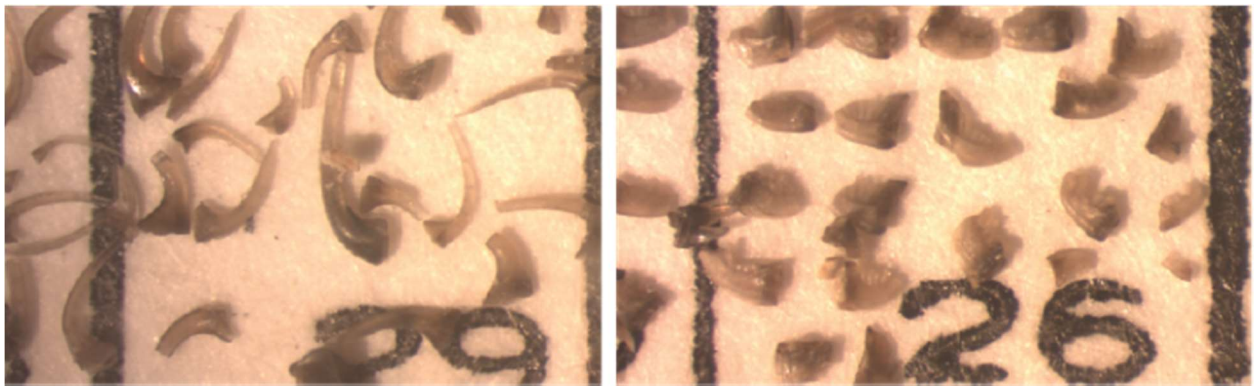

Figure 4: Representative images of conodonts related to those used for this study. These are Middle Ordovician conodonts from Oklahoma, which include those from the North American Midcontinent biogeographic realm. These include coniforms (left) and ramiforms (right), the two primary types of elements utilized by conodonts as food gathering apparatuses (Sweet and Donoghue, 2001).

Chemostratigraphy

Both $\delta^{13}C$, extracted from carbonate rock, and $^{87}Sr/^{86}Sr$, extracted from apatite in conodont elements, are utilized here to supplement the biostratigraphic information provided by the conodonts and better date the section (Saltzman et al., 2014) (Fig. 5). The $\delta^{13}C$ changes as a function of the burial of isotopically light organic matter, although other factors may play a role (Saltzman and Thomas, 2012; Edwards and Saltzman, 2014). Seawater $^{87}Sr/^{86}Sr$ changes in response to silicate weathering, with ^{87}Sr being the radiogenic daughter product of ^{87}Rb (Holmden et al., 1996; MacArthur et al., 2012). For this study, comparisons are made to $^{87}Sr/^{86}Sr$ and $\delta^{13}C$ reference curves at Clear Spring, Maryland (Saltzman and Edwards, 2017), and the global curves (MacArthur et al., 2012; Saltzman and Thomas, 2012; Saltzman et al., 2014).

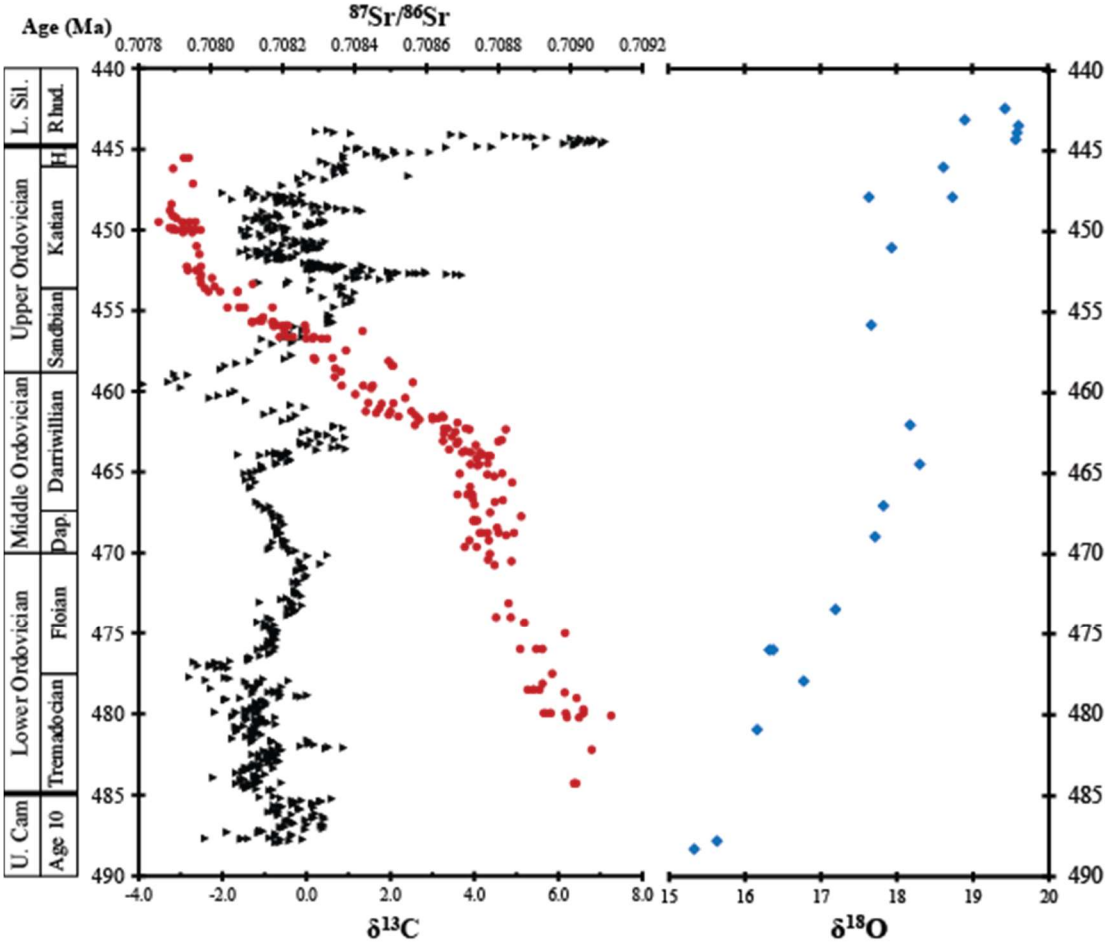

Figure 5: Composite global $^{87}Sr/^{86}Sr$ seawater curve in red circles (MacArthur et al., 2012), $\delta^{13}C$ seawater curve in black triangles (Saltzman and Thomas, 2012), and $\delta^{18}O$ in blue diamonds through the Ordovician (Trotter et al., 2008). The strontium and carbon curves contain identifiable features useful for chemostratigraphic analysis. For strontium, the rapid decrease during the Darriwilian and Sandbian likely indicates an increase in volcanic weathering (Young et al., 2009). The $^{87}Sr/^{86}Sr$ has greater variation due to the diagenetic differences between curves used, making chemostratigraphic correlation more difficult (MacArthur et al., 2012). For carbon, there are several important features, with the primary feature for this study being the positive $\delta^{13}C$ excursion during the Darriwilian. The Clear Spring data include a negative $\delta^{13}C$ excursion that does not appear in other global curves (Saltzman and Edwards, 2017). The general positive slope in the $\delta^{18}O$ indicates cooling through the early Ordovician, stabilizing around the Darriwilian (Trotter et al., 2008).

Previous Work

Unpublished work at Collierstown by Matthew Saltzman has obtained $\delta^{13}C$ values for the section being described, and is utilized within this study. Work done by Umholtz (2014) and Bloomfield (2014) studied outcroppings of the Knox Unconformity at East River Mountain, West Virginia and Rocky Gap, Virginia, both of which are in close proximity to the material utilized by the current study (Fig. 1). Dwyer and Repetski (2012) had an extensive study of the unconformity outcropping in the southern United States, specifically in northern Mississippi. Additionally, they described the occurrence of the Knox Unconformity in Central Alabama (based on Shaw et al., 1991). Dwyer and Repetski (2012) determined a wide range of lithologic information relating to the Knox Unconformity, including the range of time that the unconformity covered. The Knox Unconformity's exposure within the Black Warrior Basin was primarily confined to the *Histiodella holodentata* conodont biozone (Dwyer and Repetski, 2012), while its extent in Central Alabama's Western Facies covers most of the Lower to Middle Ordovician (Shaw et al., 1991). Several other sources have indicated similar unconformities throughout the world. Unconformities in China (Lin et al., 2012) occur in a similar timeframe to those represented by the Knox Unconformity. When comparing this to sea-level curves provided by Haq and Schutter (2008) and Nielsen (2011), several sea level regressions might correlate to these unconformities.

METHODS

Rock Sampling

Rock samples were obtained from an outcrop of the Collierstown Section described above. Eighteen samples of carbonate rock were obtained from the outcrop, all approximately 5-6 kg in weight to use for conodont extractions. Smaller hand samples were also collected for use in carbon isotope analysis.

Rock Processing for Conodont Extraction

The rock sample was processed through a rock crusher to increase the surface area of the samples. This was followed by acid bath treatment to dissolve the carbonate material. Using a dilute acetic acid solution (6%), the samples were allowed to sit for approximately three days, which is about the length of time for half of the carbonate material to be dissolved. The residue was then sieved to isolate material within the 0.125–0.250 mm range, and desiccated in a convection oven overnight until dry. A high-powered magnetic separator was used to separate magnetic materials, primarily magnetite and hematite, from non-magnetic materials, which included the conodonts. The non-magnetic material was then processed through heavy liquid separation to separate out the denser apatite and other minerals. This process utilized acetylene tetrabromide (TBE) to separate heavy material. This was followed by several rinses of acetone to reclaim the acetylene tetrabromide and remove it from the material, and left to dry overnight.

Conodont Collection

In order to obtain conodonts from the remaining residue, a microscope and fine tipped paintbrush were used. The brush was used to carefully remove conodont elements without attached material. These conodonts were closely examined to identify any important species for biostratigraphic use. In addition, color was taken and compared to the conodont alteration index to determine the degree of diagenetic alteration (based on Epstein et al., 1977). The conodonts were organized on micropaleontology slides in order to later review the material for strontium isotope extraction.

Strontium Isotope Analysis

Conodont elements that were not pertinent to biostratigraphy were then separated and weighed. Samples with sufficient mass, typically of 100μg or greater, were cleaned with 1 mL of 18 MΩ Milli-Q water in 1.5mL polypropylene centrifuge tubes (c-tubes) and rapidly shaken, with the supernatant pipetted off. This process was repeated a second time to fully clean the conodonts of any extraneous material. Samples were then dissolved in 1mL 6N HCl overnight. This process was followed by extraction of the supernatant portion and two rinses of 1 mL of 18 MΩ Milli-Q H_2O of the c-tube, each followed by repeated extraction. The extracted solution was placed into a 15mL plastic beaker containing a spiked solution of ^{84}Sr and left on a low temperature hotplate overnight. Afterwards, two elutions of 2N HCl were done through glass columns containing Bio-rad AG50 x 8, 200-400 mesh, H^+ form cation exchange resin. The eluted solutions were then placed on a hotplate overnight to remove the excess liquid.

The residue was dissolved in 10-20 μL 0.3N HCl to place in the Finnegan MAT thermal ionization mass spectrometer (TIMS) at the Radiogenic Isotope Laboratory at The Ohio State

University. Small amounts of solution were placed onto rhenium filaments and loaded onto a magazine to place in the mass spectrometer. Afterwards, air was pumped out of the mass spectrometer to produce a vacuum. The samples were then heated through the introduction of a high voltage current through the filaments. These heated samples were ionized by a second filament adjacent to filament with the samples, and pulled through the vacuum chamber with a small magnet. A powerful electromagnet then bent the beam of strontium to produce several beams, differentiated based on their different atomic masses. Measurements of these isotopes were taken based on the voltage output caused by these different beams impacting Faraday cups located at the end of the chamber, with each cup aligned to a specific atomic mass. Scans could be repeated up to 100 times per run, or until the material ran out or reached a low enough uncertainty, with outlying scans being removed during and after a single run for a sample. Outlying scans within a sample, based on degree of difference from the sample's average, were removed in order to improve the accuracy of the data obtained. The results were compared to the spiked solution of ^{84}Sr in order to determine the approximate concentration of Sr (ppm) in the material. All procedures of strontium extraction and measurement are as described by Foland and Allen (1991).

RESULTS

Conodont Biostratigraphy

The conodonts obtained from Collierstown match those found by O'Neill (1985). Overall, most of the conodonts reflect the North American Midcontinent conodont biogeographic realm, with a few representative of the North Atlantic realm (Table 1). Many of the conodonts examined are in poor condition, being nearly black in color, and can be classified on the conodont alteration index (CAI) as 3 to 5 (based on Epstein et al., 1977). Several other specimens were too fragmentary to study.

The majority of the identified specimens correlate to a range of conodont zones in the North American Midcontinent (based on Dwyer and Repetski, 2012). Elements of species, such as *Plectodina* sp., *Erismodus* sp., *Phragmodus flexuosus*, and *Curtognathus typus*, all occur throughout the studied section. These specimens are frequent and indicative of the North American Midcontinent biogeographic realm, but are poor to use for aging as they have long temporal ranges. Based on the samples available (Table 1), the New Market Limestone appears to be primarily within the *Cahabagnathus sweeti* zone. However, the lower end and underlying Beekmantown Dolomite may be *C. friendsvillensis* or older in age. Conodonts from this study that are representative of the North Atlantic would agree. Groups such as *Panderodus* sp. are as common as the groups described for the North American Midcontinent and occur throughout the section. However, these are also not diagnostic of age.

Table 1: Complete table of conodonts identified for the Collierstown section. Several samples lacked conodonts entirely (CL 1.1, CL 2.1, CL 3.2, CL 3.3) or contained many near or completely unidentifiable fragments. Conodonts such as *Plectodina* sp., *Panderodus gracilis*, *Panderodus* sp., *Erismodus* sp., *Phragmodus flexuosus*, *Phragmodus* sp., and *Curtognathus typus* were extremely common throughout the section and useful towards indicative of the biogeographic realms, but only marginally useful towards identifying the proper conodont zones. Several samples were combined for $^{87}Sr/^{86}Sr$ analysis due to the low number, and mass, of conodonts present. Additionally, two samples, CL 3.2 and CL 6.1, had additional fossilized material determined to not be conodonts, having two unidentified cone-like objects and an ostrocod, respectively.

Sample ID	CL 1.1	CL 2.1	CL 2.2	CL 3.1	CL 3.2	CL 3.3	CL 4.1	CL 4.2	CL 4.3	CL 5.1	CL 5.2	CL 5.3	CL 6.1	CL 6.2	CL 6.3	CL 7.1	CL 7.2	CL 7.3
Meters above New Market base	-1.25	1.5	2.625	4.125	6.375	7.75	9.875	13.25	15.5	20.375	22.25	23.7	27.3	35.3	37	41.4	49.4	56.3
Plectodina sp.	-	-	5	2	-	-	6	2	1	-	1	-	-	4	4	3	2	5
Besselodus variabilis	-	-	2	-	-	-	-	-	3	-	-	-	2	-	-	-	-	-
Panderodus gracilis	-	-	21	-	-	-	-	-	3	-	-	-	2	-	7	3	8	15
Panderodus sp.	-	-	-	4	-	-	-	1	5	-	-	-	-	-	-	-	-	2
*Erismodus*p.	-	-	9	4	-	-	12	2	8	6	2	-	-	4	2	10	-	3
Phragmodus flexuosus	-	-	2	2	-	-	-	-	-	-	1	-	-	-	-	-	2	1
Phragmodus sp.	-	-	-	-	-	-	-	-	2	-	-	-	-	-	-	4	-	7
Curtognathus typus	-	-	5	2	-	-	-	2	2	3	1	-	2	3	-	2	-	-
Appalachignathus delicatulus	-	-	1	-	-	-	-	-	-	1	-	-	-	-	-	-	-	-
Protopanderodus sp.	-	-	-	-	-	-	10	-	-	-	-	-	-	-	-	-	-	-
Drepanoistodus suberectus	-	-	-	-	-	-	5	-	-	-	-	-	-	-	-	-	2	-
Rhipidognathus sp.	-	-	-	-	-	-	7	-	-	-	-	-	2	8	-	3	-	-
Multioistodus subdentatus	-	-	-	-	-	-	-	-	2	2	-	-	-	-	-	3	-	-
Multioistodus sp.	-	-	-	-	-	-	3	-	-	-	-	-	1	4	-	-	-	-
Eoneoprioniodus alatus	-	-	-	-	-	-	-	-	-	-	1	-	-	2	-	5	-	-
Eoneoprioniodus sp.	-	-	-	-	-	-	-	-	-	-	-	-	-	-	-	5	-	-
Bryantodina typicalis	-	-	-	-	-	-	-	-	-	-	-	-	1	-	-	-	1	-
Walliserodus nakholmensis	-	-	-	-	-	-	-	-	-	-	-	-	-	-	1	-	-	-
Unidentified Cones	-	-	3	-	-	-	3	7	4	1	1	-	1	6	-	3	-	11
Unidentified Blades	-	-	9	-	-	-	5	5	4	-	3	1	3	3	2	4	3	3
Fragments	-	-	6	6	-	-	4	-	-	1	-	1	-	-	-	-	1	-
Unidentified	-	-	-	2	-	-	1	1	-	-	-	-	1	3	-	1	1	-
Other	-	-	-	-	2(unknown)	-	-	-	-	-	-	-	1(ostrocod)	-	-	-	-	-
Total Identified	0	0	45	14	0	0	43	7	26	12	6	0	10	25	14	38	15	33

Carbon Isotope Chemostratigraphy

The Saltzman data (unpublished) obtained for carbon isotopes spanned a larger time frame than those for strontium, being obtained through higher strata. A total of 31 $\delta^{13}C$ values were obtained out of 45 samples from near the Knox Unconformity to about 135 m above the section. These values have a range of -2.1 ‰ to 0.8 ‰ (Fig. 6). These are within the global expected values for $\delta^{13}C$. The majority of the $\delta^{13}C$ values are approximately -1.0. A positive peak occurs near the middle of the New Market Limestone, around 16–28m above the base, which reaches a $\delta^{13}C$ of +1.0 ‰. This excursion contains four data points at the peak and two additional points following at decreased values towards -1.00. Afterwards, there are minor fluctuations around -1.0 ‰ and another excursion near 120m above the base of the section that goes up to 0.0 ‰. This other peak only encompasses a single point, which might only indicate a momentary outlier.

Strontium Isotope Chemostratigraphy

Due to limited amounts of conodonts, adjacent samples were combined in some cases to fulfill the approximately 100µg minimum, creating an average value for the samples included. This occurred for samples CL 5.1-CL 5.3 (CL 5) and CL 7.2-CL 7.3 (CL 7.2-3). Including these combined samples, data was obtained from ten samples on the TIMS. Of the ten values obtained, two were removed due to high uncertainty (CL 4.3 and CL 6.3), primarily caused by a low mass of conodonts (not enough Sr). The remainder indicate a range of $^{87}Sr/^{86}Sr$ from 0.70816 to 0.70865 (Fig. 6). Most uncertainties for the remaining samples are less than $2.5x10^{-5}$, which is similar to the external reproducibility, based on SRM 987 standard. Of the remaining eight samples, two were above this uncertainty but below $6x10^{-5}$, CL 4.2 and CL 7.2-3 (for all values obtained, see appendix).

The data show decreasing values as you move up the strata. Sample CL 2.2, the lowest sample stratigraphically, also has the highest $^{87}Sr/^{86}Sr$ ratio, at 0.70865. The highest sample, CL 7.2-3, has a value of 0.70842. The majority of the remaining data fits within these two with slight variation, with $^{87}Sr/^{86}Sr$ exhibiting decreasing values during the period being studied. Sample CL 6.2 is a slight outlier compared to the remainder of the dataset, but is comparable to the variability seen in many studies of $^{87}Sr/^{86}Sr$ for this age (MacArthur et al., 2012; Saltzman et al., 2014). This follows a negative trend of $-6x10^{-6}$ for the $^{87}Sr/^{86}Sr$ per meter above the base of the New Market formation, with this base itself being estimated at 0.70860 based on this trend.

Figure 6: Collierstown $^{87}Sr/^{86}Sr$ and $\delta^{13}C$ seawater curves with sample locations and formations present, including lithology. Previous work indicates a *Pygodus serra* to *P. anserinus* conodont zones for the formation, within the North Atlantic realm (O'Neill, 1985), which approximately corresponds to the *Cahabagnathus friendsvillensis* to *C. sweeti* conodonts zones of the Midcontinent (Bergström et al., 2009). A general negative slope, represented by the line, is present for the $^{87}Sr/^{86}Sr$ curve, while the primary feature in the $\delta^{13}C$ curve is a positive excursion by a few points. The range of values seen by the $^{87}Sr/^{86}Sr$ and the rate of the negative slope indicate an early part of the change seen in the Darriwilian (Young et al., 2009), approximately around 463 Ma for the lowest most point. The positive $\delta^{13}C$ excursion seen in the carbon most closely resembles the Darriwilian one seen in Saltzman and Thomas (2012) based on the size and span of the excursion. The peak slightly plateaus around 1.0, 2 points higher than the general decrease during this time. It should also be noted that material for $\delta^{13}C$ was gathered higher up into the section than what was obtained for $^{87}Sr/^{86}Sr$, though this contains little consequential data to the current study.

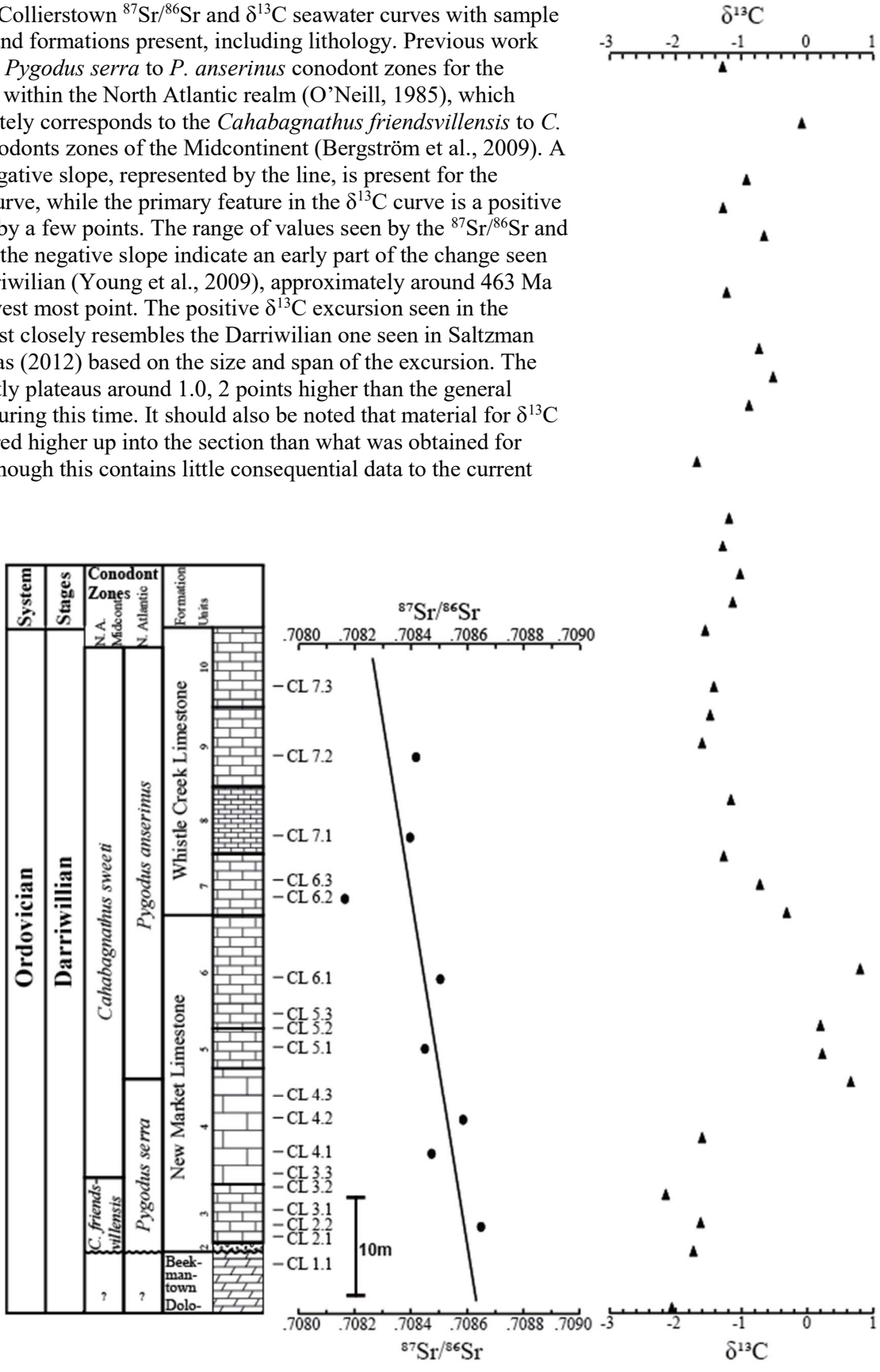

Discussion

Because biostratigraphy is insufficient to conclude a proper age for the Knox Unconformity, $^{87}Sr/^{86}Sr$ and $\delta^{13}C$ seawater isotope curves were obtained for chemostratigraphic correlation. New data for the Collierstown section are useful in dating the Knox Unconformity, and show that the timing is comparable to other surfaces in the region and around the world. In addition, the combination of isotopic seawater curves as well as sea-level changes has important implications for causes of the evolutionary radiations of the GOBE.

Biostratigraphic Dating

O'Neill (1985) described the New Market Limestone in the Collierstown section as Middle Ordovician in age, and the conodonts identified in this study agree. O'Neill (1985) described conodonts that spanned the *Pygodus serra* to *P. anserinus* conodont zones of the North Atlantic biogeographic realm, which is approximately equivalent to the *Cahabagnathus sweeti* to *C. friendsvillensis* conodont zones of the North American Midcontinent. These zones indicate the New Market Limestone falls largely within the Darriwilian stage of the Ordovician.

Few age diagnostic fossils are present within the Collierstown section to determine an age conclusively. Several identified conodont elements have long ranges, and the overlapping of approximate ranges provides a general age for the section (Table 1). Additionally, the general quality of the conodont elements within this section is poor. Many of the elements are fragmentary, even those that could be identified based on key characteristics. Most of the elements had a CAI of 3 to 5 (based on Epstein et al., 1977), which is indicative of heat alteration of 100°C–300°C. It is likely that conodonts from the lower formation, the Beekmantown Dolomite, were reworked into the lower portions of the New Market Limestone, which would also diminish the accuracy of biostratigraphic dating (O'Neill, 1985), though this is hard to determine due to the lack of age-diagnostic specimens.

Chemostratigraphic Refinement

The chemostratigraphic analysis of stable carbon isotopes ($\delta^{13}C$) helps provide insight into the age. There are several large $\delta^{13}C$ excursions throughout the Ordovician (Saltzman and Thomas, 2012). Based on the global carbon seawater curve (Fig. 5), the Ordovician is generally around $\delta^{13}C$ of -1.0 ‰, but several major excursions include major positive peaks of 1.0 ‰ around mid-Darriwilian, 4.0 ‰ at the beginning of the Katian, and nearly 8.0 ‰ at the end of the Ordovician (Bergström et al., 2009). Additionally, there is a major negative $\delta^{13}C$ noted at Clear Spring, MD, a local reference curve, though this is absent in other $\delta^{13}C$ curves such as the one seen in Baltoscandia (Saltzman and Edwards, 2017).

Of these different excursions, the one that most closely matches the results obtained is the positive $\delta^{13}C$ peak around the middle of the Darriwilian age, at approximately 462.5 Ma (Fig. 6). Not only does this match the timeframe set down by the biostratigraphy, but also the $\delta^{13}C$ rise is equivalent, reaching up to approximately 1.0 ‰. In the local reference curve at Clear Spring, there is an immediate drop following this positive excursion that reaches -4.0 ‰, which does not show up in the Collierstown section. However, this lack of a negative $\delta^{13}C$ excursion does match up with the seawater $\delta^{13}C$ curve seen elsewhere in the world (Saltzman and Edwards, 2017).

Global and local carbon cycling can affect $\delta^{13}C$ (Edwards and Saltzman, 2014). This makes use of the $\delta^{13}C$ seawater curve at Clear Spring difficult because the positive $\delta^{13}C$ peak

may be global and accurate, but the negative $\delta^{13}C$ excursion may indicate a local signal not present at Collierstown. In addition, the reworking of the lower portions of the New Market Limestone, as described by O'Neill (1985), may have affected the continuity of the $\delta^{13}C$ trends at Collierstown. Therefore, the base of the New Market Limestone and occurrence of the Knox Unconformity can only be tentatively placed around 463 Ma based on $\delta^{13}C$.

With the $\delta^{13}C$ seawater curve generally reinforcing the biostratigraphy, the $^{87}Sr/^{86}Sr$ may help refine the age for the end of the Knox Unconformity. The $^{87}Sr/^{86}Sr$ of Saltzman et al. (2014) was utilized as a global reference (see also MacArthur et al., 2012; Saltzman and Edwards, 2017). A trend toward less radiogenic values occurs throughout the Ordovician, and increases in rate from midway through the Darriwilian through the Sandbian (Fig. 5).

The $^{87}Sr/^{86}Sr$ values obtained in this study indicate that the Knox Unconformity terminated immediately following the increase in the rate of fall of $^{87}Sr/^{86}Sr$. The highest values, near 0.7086 in the basal New Market, represent values observed before the rate of fall increases (Fig. 6). The values of 0.7084 at the top of the section date the New Market and Whistle Creek Limestones at approximately 462.5 Ma (Fig. 7).

The $^{87}Sr/^{86}Sr$ does not definitively address the age of the Knox Unconformity because there is noise in the dataset. There is the small possibility of analytical uncertainty, on the scale of 10^{-5}, though this is reduced through the removal of high uncertainty outliers. Additionally, diagenetic processes may cause alterations in the chemistry of the conodonts, such as seen with the heat alteration that affects most of the elements described, although this is unlikely to affect the $^{87}Sr/^{86}Sr$ (Epstein et al., 1977). More likely, the introduction of more radiogenic material over time might increase the $^{87}Sr/^{86}Sr$ (Saltzman et al., 2014). Though this is a possibility, it is also important to note that the scatter in the global reference curve being utilized (MacArthur et al., 2012) decreases the degree of correlating Collierstown to the global curve. However, the collaboration of all three methods, places a high likelihood that the base of the New Market Limestone is around 462.5 Ma.

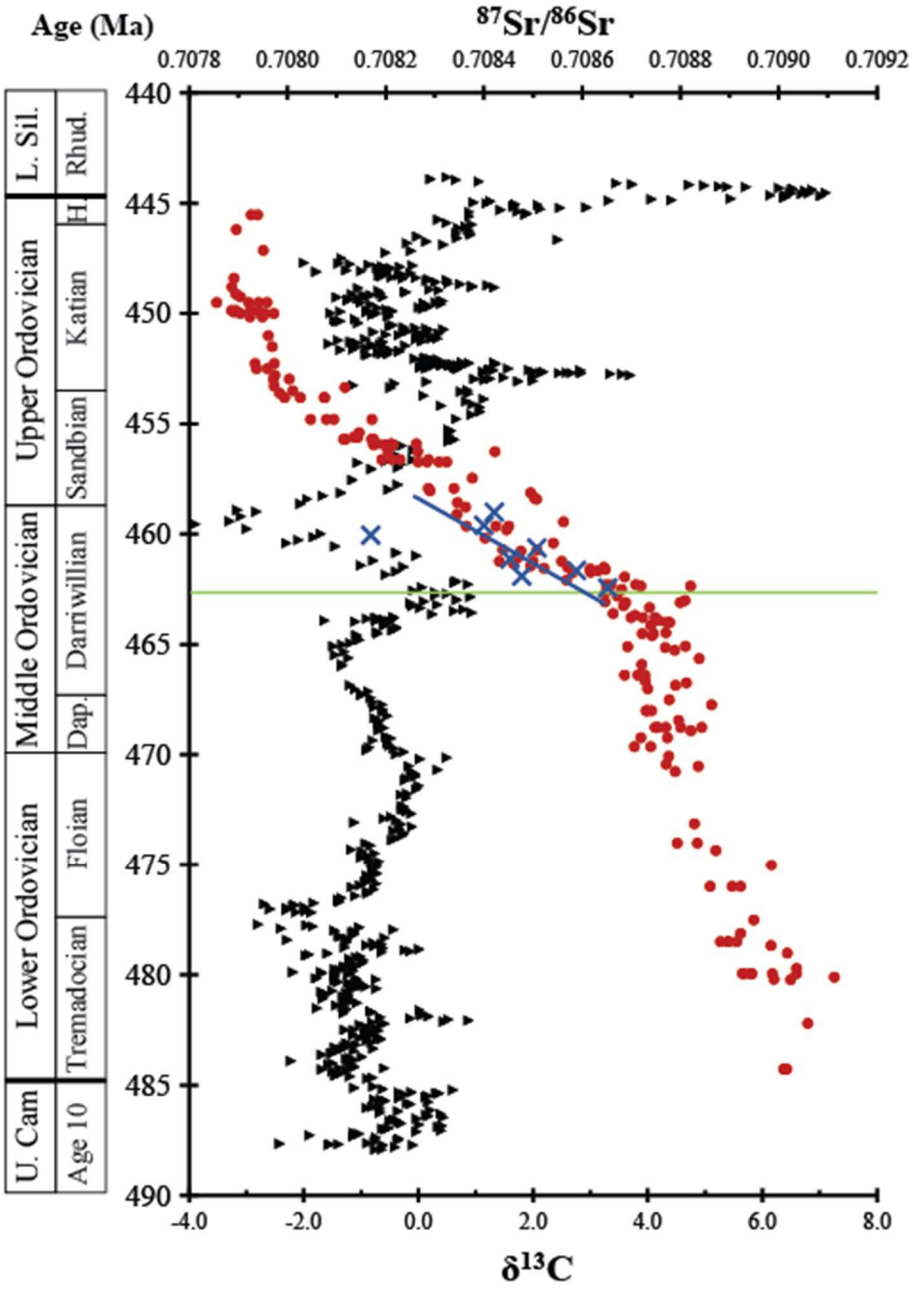

Figure 7: Collierstown $^{87}Sr/^{86}Sr$ overlain onto the global seawater strontium reference curve (MacArthur et al., 2012). The red circles represent Ordovician $^{87}Sr/^{86}Sr$; the black triangles represent Ordovician $\delta^{13}C$ (as seen in Fig. 5). The blue represents the trend-line determined for the Collierstown $^{87}Sr/^{86}Sr$, depicted as blue X's, and is matched up to the global curve. The green line indicates the base of the New Market Limestone, and therefore the top of the Knox Unconformity. This places the end of the unconformity around 462.5 Ma. The date obtained for the unconformity based on $^{87}Sr/^{86}Sr$ bisects the positive $\delta^{13}C$ excursion, which is clearly seen in the Collierstown section.

Does the Knox Unconformity represent a global event?

Umholtz (2014) described two sections within the central Appalachians, East River Mountain, West Virginia and Rocky Gap, Virginia, with additional work done by Bloomfield (2014) on the former (Fig. 1). Material at or below the unconformity at Rocky Gap indicate ages, based on $^{87}Sr/^{86}Sr$, of approximately early to middle Floian, with $^{87}Sr/^{86}Sr$ values in the Blackford formation above indicating a late Darriwilian age within the *C. friendsvillensis* to *C. sweeti* zones, supported by $\delta^{13}C$ (Umholtz, 2014). On the other hand, East River Mountain's $^{87}Sr/^{86}Sr$ indicates an age of approximately 466.5 Ma before the unconformity and 456.5 Ma above the unconformity (Bloomfield, 2014). However, this 10 Ma gap lacks many intermediate samples within its study, and, therefore, Bloomfield (2014) indicates a likely shorter timespan for the East River Mountain unconformity. This indicates some local variation in the timing of sea-level regression. Unfortunately, the strata at the top of the Knox Dolomite at Collierstown lacked usable conodont material, making the length of the sea-level fall difficult to determine.

Another section containing the Knox Unconformity comes from Dwyer and Repetski (2012), which occurs in Alabama and Mississippi. An analysis of the Black Warrior Basin material in Mississippi found that the unconformity's occurrence primarily occupied the *H. holodentata* conodont zone within the Darriwilian (Dwyer and Repetski, 2012). This occurs within the time range described by Umholtz (2014), coinciding with the approximate beginning described by Bloomfield (2014). However, the Collierstown data indicate an end that is far later, occurring within the *C. friendsvillensis* zone. Dwyer and Repetski's (2012) analysis in Central Alabama indicate the Knox Unconformity in eastern facies occupied most of the early Middle Ordovician, while the western facies indicate the unconformity began in the Upper Cambrian and continued until the beginning of the Upper Ordovician (Dwyer and Repetski, 2012, based on Shaw et al., 1991). This extensive length of time for the Knox Unconformity likely represents erosion into underlying strata.

In the Tarim Basin in western China, Lin et al. (2012) described two areas, Tabei and Tazhong, within the Tarim Basin and determined what factors influenced the depositional sequences of this region. There are two regressions present in the Tarim Basin, one at the onset of the Darriwilian and one at its conclusion. These two are within the ranges described by other North American sections for the Knox Unconformity, such as the Black Warrior Basin and East River Mountain, yet are not indicative of the transgression that terminated the Knox Unconformity at Collierstown, which is dated to the middle Darriwilian. However, Lin et al. (2012) also described tectonic activity occurring during this interval that could explain the regression seen within China. During the Middle Ordovician, this region began to experience compression, with low relief faulting (Wang 2004). This orogenic event subsided the basin, resulting in the lack of a transgression in the area being studied (Lin et al., 2012).

Nielsen (2011) described a sea-level curve for the Ordovician of Baltoscandia while Haq and Schutter (2008) created a global sea-level curve for the Paleozoic (Fig. 8). In Baltoscandia, there are several sea-level regressions which occur throughout the Darriwilian, with major drops occurring around 465.5 and 462 Ma, the latter coming after a large transgression (Nielsen, 2011). This local sea-level transgression is correlated to the value determined for the Collierstown outcropping of the Knox Unconformity.

In a comparison of the Collierstown section to the global sea-level curve developed by Haq and Schutter (2008), there was a distinct regression followed by rapid transgressions around 462.8 Ma, which is within the realm determined for the upper limit of the Knox Unconformity at Collierstown, 462.5 Ma. Many outcroppings of the Knox Unconformity contain multiple unconformities (Fig. 8) possibly implying repeated regressions and transgressions (Dwyer and Repetski, 2012; Umholtz, 2014; Bloomfield 2014). Haq and Schutter's (2008) global sea-level curve also shows multiple regressions within the later Darriwilian.

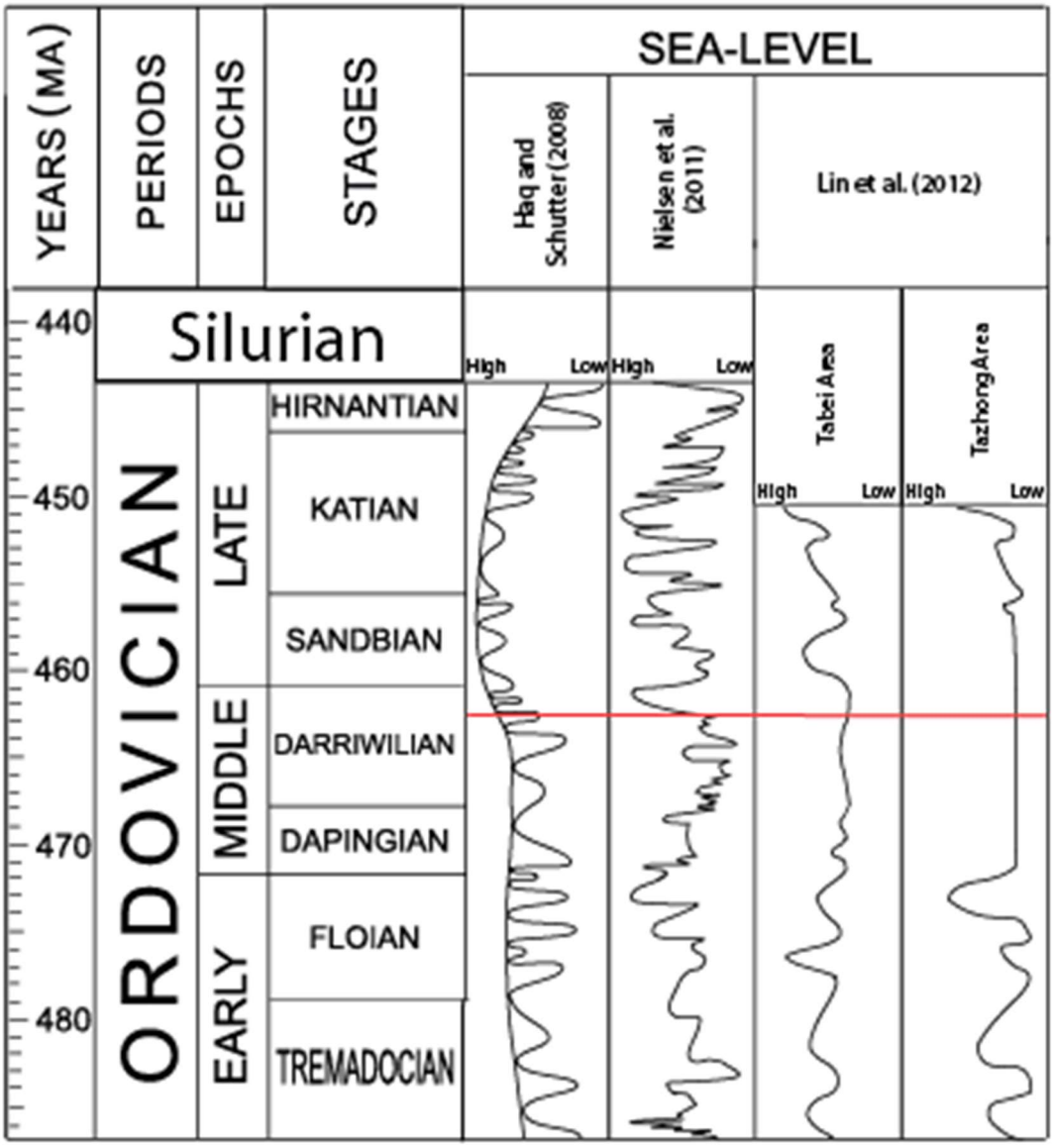

Figure 8: Sea level curves for the Ordovician. Haq and Schutter (2008) provide an approximate global sea-level curve, Nielsen et al. (2011) provide a local sea-level curve for Baltoscandia, and Lin et al. (2012) provide two local sea-level curves around the Tarim Basin, with far lower resolution. The general trend is high sea levels, with several fluctuations, partially due to temperature (Haq and Schutter, 2008). The red line indicates the derived timing of the termination of the Knox Unconformity at Collierstown, 463Ma, based on this study. It is comparable to transgressions seen in Baltoscandia (based on Nielsen et al., 2011) and the global sea-level curve (Haq and Schutter, 2008).

Implications for climate and the Great Ordovician Biodiversification Event (GOBE)

The changes that led to the formation of the Knox Unconformity indicate tectonic uplift or glacial ice buildup that affected climate and life. The Taconic Orogeny represents mountain building processes that increased weathering rates and provided nutrients into the ocean (Mussman and Read, 1986). Lin et al. (2012) provided insight into orogenic activity in another region of the world at the same time.

The change from 0.70865 to 0.70842 probably indicates a decrease in weathering of high $^{87}Sr/^{86}Sr$ rocks, which relates to the submergence of radiogenic sources, likely through eustatic rise in sea-level, or weathering of basaltic (non-radiogenic) volcanic material during the Taconic Orogeny (Young et al., 2009). Higher rates of weathering liberate calcium ions from the volcanic material to lock up CO_2 in $CaCO_3$, reducing atmospheric greenhouse gases and decreasing the global temperature (Berner, 2006).

Although high degrees of biodiversification are typically associated with warmer climates (Harper et al., 2015), the cooler periods seen throughout the Ordovician may have led to sea surface temperatures similar to the modern sea surface temperatures and therefore greater degrees of evolution due to the temperature tolerances of marine faunal groups (Trotter et al., 2008). The evidence obtained by this study, the sea-level regression represented by the Knox Unconformity, corresponds to the $\delta^{18}O$ and corroborates this model for the GOBE.

CONCLUSIONS

The Knox Unconformity at Collierstown, Virginia, represents a sea-level regression that terminated approximately 462.5 Ma. This conforms to the range prescribed by previous biostratigraphic work done on the section (O'Neill, 1985). It also presents a similar age to that found by Umholtz (2014), though being older than material described by Bloomfield (2014). This fits into the range of possibilities seen for the Knox Unconformity in the southern United States, but occurring later than the Black Warrior Basin's unconformity (Dwyer and Repetski, 2012). Most distinctly, the regression represented by the Knox Unconformity matches with the global sea-level drop described by Haq and Schutter (2008) around 462.8 Ma.

The presence of the Knox Unconformity and many other regressions are highly indicative of a fluctuating sea-level which likely had major impacts on climate, and therefore the rate of evolution throughout the Ordovician. The $^{87}Sr/^{86}Sr$ record for this section matches that for the global seawater curve (Saltzman et al., 2014). This indicates increased weathering of volcanic material, which removes CO_2 from the atmosphere and therefore is a proxy for decreasing temperature and increasing rates of sea-floor spreading. This is backed by the $\delta^{18}O$, which indicates a general cooling trend throughout the Early to Middle Ordovician (Trotter et al., 2008), while sea-levels climb throughout the first half of the Ordovician (Haq and Schutter, 2008). All of these factors provide evidence for cooling processes affecting the GOBE.

Suggestions for Future Work

At Collierstown, it would be fruitful to obtain several samples from the top of the Beekmantown Dolomite. This formation is beneath the Knox Unconformity, providing a better age range on the length of this erosional environment, and indicating possible sources of error from material reworked into the New Market formation. The exploration of other outcroppings of the Knox Unconformity and correlated disconformities throughout the world would aid in the understanding of events occurring around this specific period of sea-level fluctuation. Greater analysis of the relationship of these Middle Ordovician disconformities to changes in sea level and global climate would be an additional step to enhance the understanding of major adaptive radiation events, as well as determine other factors involved in their formation.

REFERENCES CITED

Ainsaar, L., Kaljo, D., Martma, T., Meidla, T., Männik, P., Nõlvak, J., Tinn, O., 2010. Middle and Upper Ordovician carbon isotope chemostratigraphy in Baltoscania: A correlation standard and clues to environmental history. Palaeogeography, Palaeoclimatology, Palaeoecology 294, 189-201.

Bergström, S.M., Chen, X., Gutiérrez-Marco, J.C., Dronov, A., 2009. The new chronostratigraphic classification of the Ordovician System and its relations to major regional series and stages and to δ13C chemostratigraphy. Lethaia 42, 97-107.

Berner, R.A., 2006. Inclusion of the weathering of volcanic rocks in the GEOCARBSULF model. American Journal of Science 306, 295-302.

Blakey, R.C., 2011. Middle Ordovician mollewide plate tectonic map. http://cpgeosystems.com/470moll.jpg.

Bloomfield, C., 2014. Isotope geochemical analysis of strontium in conodont apatite: Implications for global cooling and the timing of the Middle Ordovician Knox Unconformity [B.S. thesis]. Columbus, Ohio State University, 28 p.

Cramer, B.D., Brett, C.E., Melchin, M.J., Männik, P., Kleffner, M.A., Mclaughlin, P.I., Loydell, D.K., Munnecke, A., Jeppsson, L., Corradini, C., Brunton, F.R., Saltzman, M.R., 2010. Revised correlation of Silurian Provincial Series of North America with global and regional chronostratigraphic units and $\delta^{13}C_{carb}$ chemostratigraphy. Lethaia 44, 185-202.

Dwyer, G.S., Repetski, J.E., 2012. The Middle Ordovician Knox Unconformity in the Black Warrior Basin. In: Derby, J.R., Fritz, R.D., Longacre, S.A., Morgan, W.A., Sternbach, C.A. (eds), The geology and economic resources of the Cambrian-Ordovician Sauk megasequence of Laurentia, American Association of Petroleum Geologists Memoir 98, 345-356.

Edwards, C.T., Saltzman, M.R., 2014. Carbon isotope ($\delta^{13}C_{carb}$) stratigraphy of the Lower-Middle Ordovician (Tremadocian-Darriwillian) in the Great Basin, western United States: Implications for global correlation. Palaeogeography, Palaeoclimatology, Palaeoecology 399, 1-20.

Epstein, A.G., Epstein, J.B., Harris, L.D., 1977. Conodont color alteration: An index to organic metamorphism. Geological Survey Professional Paper 995.

Foland, K.A., Allen, J.C., 1991. Magma sources for Mesozoic anorogenic granites of the White Mountain magma series, New England, USA. Contrib. Mineral Petrol. 109, 195-211.

Haq, B.U., Schutter, S.R., 2008. A chronology of Paleozoic sea-level changes. Science 322, 64-68.

Harper, D.A.T., Zhan, R., Jin, J., 2015. The Great Ordovician Biodiversification Event: Reviewing two decades of research on diversity's big bang illustrated by mainly brachiopod data. Palaeoworld 24, 75-85.

Holmden, C., Creaser, R.A., Muehlenbachs, K., Bergström, S.M., Leslie, S.A., 1996. Isotopic and elemental systematics of Sr and Nd in 454 Ma biogenic apatites: implications for paleoseawater studies. Earth and Planetary Science Letters 142, 425-437.

Lenton, T.M., Crouch, M., Johnson, M., Pires, N., Dolan, L., 2012. First plants cooled the Ordovician. Nature Geoscience 5, 86-88.

Lin, C., Yang, H., Liu, J., Rui, Z., Cai, Z., Li, S., Yu, B., 2012. Sequence architecture and the depositional evolution of the Ordovician carbonate platform margins in the Tarim Basin and its response to tectonism and sea-level change. Basin Research 24, 559-582.

MacArthur, J.M., Howarth, R.J., Shields, G.A., 2012. Strontium isotope stratigraphy. In: Gradstein, F.M., Ogg, J.G., Schmitz, M., Ogg, G. (Eds.), the Geologic Time Scale, pp. 127-144.

Mussman, W.J., Read J.F., 1986. Sedimentology and development of a passive- to convergent-margin unconformity: Middle Ordovician Knox Unconformity, Virginia Appalachians. Geological Society of America Bulletin 97, 282-295.

Nielsen, A.T., 2011. A re-calibrated sea-level curve for the Ordovician of Baltoscandia. In Gutiérrez-Marco, C.J., Rábano, I., Garcia-Bellido, D. (Eds.), Ordovician of the World: 11th Ordovician Symposium on the Ordovician System: Madrid Instituto Geológico y Minero de España 14, pp. 399-401.

O'Neill, B.E., 1985. Conodont biostratigraphy and paleoecology in the lower Middle Ordovician of the Valley and Ridge Overthrust Region of West Central Virginia [B.S. thesis]. Columbus, Ohio State University, 202 p.

Rasmussen, C.M.O., Ullman C.V., Jakobsen, K.G., Lindskog, A., Hansen, J., Hansen, T., Eriksson, M.E., Dronov, A., Frei, R., Korte, C., Nielsen, A.T., Harper, D.A.T., 2016. Onset of main Phanerozoic marine radiation sparked by emerging Mid Ordovician icehouse. Scientific Reports 6(18884), 1-9.

Read, J.F., 1980. Carbonate ramp-to-basin transitions and foreland basin evolution, Middle Ordovician, Virginia Appalachians. American Association of Petroleum Geologists Bulletin 64(10), 1575-1612.

Saltzman, M.R., Thomas, E., 2012. Carbon Isotope Stratigraphy. In: Gradstein, F.M., Ogg, J.G., Schmitz, M., Ogg, G. (Eds.), the Geologic Time Scale, pp. 207-232.

Saltzman, M.R., Edwards, C.T., Leslie, S.A. Dwyer, G.S., Bauer, J.A., Repetski, J.E., Harris, A.G., Bergström, S.M., 2014. Calibration of a conodont apatite-based Ordovician $^{87}Sr/^{86}Sr$ curve to biostratigraphy and geochronology: Implications for stratigraphic resolution. Geological Society of America Bulletin 126(11/12), 1551-1568.

Saltzman, M.R., Edwards, C.T., 2017. Gradients in the carbon isotopic composition of Ordovician shallow water carbonates: A potential pitfall in estimates of ancient CO_2 and O_2. Earth and Planetary Science Letters 464, 46-54.

Sepkoski, J.J., 1995. The Ordovician radiation: Diversification and extinction shown by global genus-level taxonomic data. Ordovician Odyssey: Short Papers for the Seventh International Symposium on the Ordovician System, Pacific Section, Society for Sedimentary Geology, pp. 393-396.

Shaw, T.M., Roberson K.E., Harris, A.G., 1991. Lithostratigraphy and conodont biostratigraphy across the Lower-Middle Ordovician disconformity (early to middle Whiterockian) at

Pratt Ferry, central Alabama. In: Sando, W.J. (Ed.), Shorter Contributions to Paleontology and Stratigraphy: U.S. Geological Survey Bulletin 1895, pp. C1-C13.

Sweet, W.C., Donoghue, P.C.J., 2001. Conodonts: Past, present, future. Journal of Paleontology 75(6), 1174-1184.

Trotter, J.A., Williams, I.S., Barnes, C.R., Lécuyer, C., Nicoll, R.S., 2008. Did cooling oceans trigger Ordovician biodiversification? Evidence from conodont thermometry. Science 321, 550-554.

Umholtz, N.M., 2014, Middle to Late Ordovician $\delta^{13}C$ and $^{87}Sr/^{86}Sr$ stratigraphy in Virginia and West Virginia: Implications for the timing of the Knox Unconformity [M.S. thesis]: Columbus, Ohio State University, 55 p.

Wang, Z.M., 2004. Tectonic evolution of the western Kunlun orogenic belt, western China. Journal of Asian Earth Science 24(2), 153-161.

Young, S.A., Saltzman, M.R., Foland, K.A., Linder, J.S, Kump, L.R., 2009. A major drop in seawater $^{87}Sr/^{86}Sr$ during the Middle Ordovician (Darriwilian): Links to volcanism and climate? Geology 37(10), 951-954.

37.768344, -79.566596. Google Street View. May 2009. 2 February 2017.

APPENDIX

Rock and Sr Sample Data

Sample ID	ticket #	meters above base of New Market	Unit (O'Neill)	Weight (kg)	Formation	Sr (ppm)	87Sr/86Sr		unc	ppm	Field Notes
1.1	427903	-1.25	1	4.74	Beekmantown Dolomite						under dead stump, dolomite, highly weathered below unconformity - unconformity approximately large flat surface between 1.1 and 2.1 where rock highly weathered, conglomerate with some angular chert
2.1	427904	1.5	3	5	New Market Limestone						fine-grained limestone, some yellow discoloration due to weathering, mostly light gray
2.2	427905	2.625	3	4.9	New Market Limestone	6075	0.708650	±	0.000019	27	fine-grained limestone, mostly light-gray, weathered surfaces darker gray
3.1	427906	4.125	3	4.12	New Market Limestone						fine-grained limestone, light gray where exposed, dark gray where weathered, some slight lamination
3.2	427907	6.375	3	5	New Market Limestone						fine-grained limestone, mostly dark gray, appears more heavily eroded, then other layers, some areas very dark and chipping, possibly some calcareous mudstone
3.3	427908	7.75	4	>5	New Market Limestone						fine-grained limestone, mostly dark gray, lighter gray on exposed surfaces, highly-chipping below, stronger lamination above
4.1	427909	9.875	4	>5	New Market Limestone	8963	0.708474	±	0.000021	30	fine-grained limestone, light gray to yellow where weathered, dark gray where exposed, some lamination appears to occur
4.2	427910	13.25	4	>5	New Market Limestone	7250	0.708586	±	0.000034	48	fine-grained limestone, light gray to yellow where weathered, more eroded from top than surrounding layers
4.3	427911	15.5	4	>5	New Market Limestone	21757	0.707344	±	0.000093	131	fine-grained limeston, light gray where weathered, edge of highly eroded top area
5.1	427912	20.375	5	>5	New Market Limestone	7218	0.708450	±	0.000019	27	fine-grained limestone, light gray to yellow where weathered, certain areas appear white
5.2	427913	22.25	5	>6	New Market Limestone						fine-grained limestone, very light gray on exposed surfaces, chipped areas appear dark-gray, light gray where weathered, some lamination present
5.3	427914	23.7	6	>5	New Market Limestone						fine-grained limestone, light gray where exposed, chipped areas somewhat dark-gray, gray where weathered
6.1	427915	27.3	6	>5	New Market Limestone	7147	0.708505	±	0.000019	27	fine-grained limestone, light gray where exposed, gray where weathered, heavily covered in vines and roots, more thinly bedded than most
6.2	427916	35.3	6	>6	New Market Limestone	9939	0.708166	±	0.000012	17	fine-grained limestone, light gray where exposed, gray where weather, some lamination above (collected slightly up in section from described location)
6.3	427917	37	6	>6	New Market Limestone	12698	0.707928	±	0.000061	86	fine-grained limestone, dark gray where chipped, lighter gray where exposed, weathering is gray, fossils in layer above
7.1	427918	41.4	7	>5	Whistle Creek Limestone	9802	0.708397	±	0.000014	20	rougher packstone, light gray in appearance, brown where weathered, weathering causes sponge-like texture, some fossils present
7.2	427919	49.4	9	>5	Whistle Creek Limestone	5269	0.708419	±	0.000054	76	rougher packstone, easily eroded, contains chert nodules and ribbons, contains calcite veins, indented (more easily weathered) than surrounding layers
7.3	427920	56.3	10	>5	Whistle Creek Limestone						rougher packstone, more eroded than surroundings, filled with calcite veins, some chert nodules, underneath bush with many branches (vine-like)